Journal of Catalysis 327 (2015) 78–85

Contents lists available at ScienceDirect

Journal of Catalysis

journal homepage: www.elsevier.com/locate/jcat

Biochemical composite synthesized by stepwise crosslinking: An efficient platform for one-pot biomass conversion

Wei Wei [a], Cong Wang [a], Yu Zhao [a], Shichao Peng [a], Haoyang Zhang [a], Yipeng Bian [a], Hexing Li [a], Xinggui Zhou [b], Hui Li [a,*]

[a] The Education Ministry Key Lab of Resource Chemistry and Shanghai Key Laboratory of Rare Earth Functional Materials, Shanghai Normal University, Shanghai 200234, PR China
[b] State Key Laboratory of Chemical Engineering, East China University of Science and Technology, Shanghai 200237, PR China

ARTICLE INFO

Article history:
Received 16 March 2015
Revised 18 April 2015
Accepted 20 April 2015

Keywords:
Biochemical composite
Yolk–shell nanostructure
Metallic catalysis
Enzymatic catalysis
Biomass conversion

ABSTRACT

This paper describes the development of a new bifunctional catalyst system that integrates enzyme and chemical material into a biochemical composite through a stepwise crosslinking approach. The as-prepared biochemical composite not only allows "one-pot" biomass conversion *via* sequential enzyme-catalyzed hydrolysis of biomass materials to glucose and metal-catalyzed hydrogenation of glucose to sorbitol, but also enables reusability of the catalyst. This design concept facilitates access to fuels and chemicals from the biomass-derived sorbitol and will attract more attention in the foreseeable future.

1. Introduction

The production of fuels and chemicals from plentiful and renewable biomass resources has drawn immense attention in recent years [1–5]. Sorbitol, a hexitol, is a valuable platform chemical that can be converted by straightforward methods into a variety of useful products [6]. Nowadays, almost all extant sorbitol production processes are usually based on the hydrogenation of glucose catalyzed by metallic catalysts [7–13]. In fact, glucose can be facilely obtained from biomass materials, primarily starch [14–16] and even cellulose, [17] through enzymatic hydrolysis bioprocesses. Apparently, a combined, one-pot hydrolysis–hydrogenation of biomass materials to sorbitol displays some advantages in its step-saving and low costs mainly linked to both the separation and the refining procedures [18–20]. Nevertheless, our previous studies revealed the one-pot process contains incompatible parameters. More specifically, enzymes are easily poisoned when contacting with metal catalysts, while metallic active sites would be covered by enzymes and the colloidal substances originated from hydrolysis of biomass materials, leading to a rapid deactivation for the subsequent glucose hydrogenation. Noting that encaging a functional material within another material can form a yolk–shell configuration that provides protecting effect on the individual core [21], very recently, we designed yolk–shell nanoarchitectures consisting of cores made of supported Ru encapsulated within porous silica shells [22,23]. By combining such materials with amyloglucosidase, one-pot hydrolysis–hydrogenation of dextrin has been successfully conducted to produce sorbitol where the porous silica shell separates the incompatible catalysts in different regions. Specifically, the enzymatic hydrolysis of dextrin to glucose occurs outside the yolk–shell nanoarchitectures owing to the blocking effect of the silica shells on the large enzyme molecules. Meanwhile, the permeation-selective porous silica shells offer a convenient path for the produced small glucose molecules crossing into the catalytically active cores for hydrogenation to sorbitol. While promising, the present process still uses free enzyme which decreases the economical attractiveness owing to the difficulty associated with the reusability of enzyme and the protein contamination of the final product. Therefore, immobilization of enzyme directly onto the outer surface of shell is needed to ensure the achievement of a real merging of such yolk–shell nanostructures and enzyme.

With advances in material science, a number of techniques have been developed for enzyme immobilization, such as support binding (physical binding, ionic binding, or covalent binding), entrapment, and crosslinking [24]. To enhance the operational stability and reusability of amyloglucosidases for bioprocessing,

* Corresponding author. Fax: +86 21 64322272.
E-mail address: lihui@shnu.edu.cn (H. Li).

http://dx.doi.org/10.1016/j.jcat.2015.04.021
0021-9517/

they have been immobilized *via* various methods by far. Using polyethyleneimine-coated sepabeads as supports, Torres et al. successfully immobilized glucoamylase *via* ionic adsorption [25]. In comparison with ionic binding, covalent binding of enzyme to insoluble carriers is even stronger. In 2008, Kamal et al. reported the covalently immobilization of glucoamylase on polypropylene-grafted fibers by using carbodiimide as a coupling agent [26]. By using glutaraldehyde [27] or polyglutaraldehyde [28] as coupling agent, amyloglucosidase was attached to silanized magnetic nanoparticles or gelatin. Compared to other coupling agents, glutaraldehyde-based coupling reaction requires mild conditions. In those reports, immobilized amyloglucosidases were found to be more beneficial relative to the corresponding free enzymes. Despite the well-known advantages for enzyme immobilization, the immobilization of amyloglucosidase has not been performed frequently in industrial because the macromolecular enzyme loading is still a tough issue. Crosslinking technique has proved to be a promising approach for carrier-free immobilization of enzyme, which permits multipoint attachment through intermolecular crosslinking between enzyme molecules [29]. Based on this technique, Talekar et al. recently developed a combi-CLEAs strategy to prepare carrier-free co-immobilization of macromolecular enzymes, glucoamylase, and pullulanase [30]. In our research, we sought to address these concerns by *both* covalently attaching of yolk–shell nanostructures onto amyloglucosidase *and* ensuring an insoluble and robust biochemical catalyst.

Herein, we design a recyclable bifunctional biochemical composite. The synthesis of such composite is achieved through a stepwise crosslinking method that involves the covalent attachment of yolk–shell structured chemical catalyst onto amyloglucoamylase with glutaraldehyde and the subsequent coupling of the composite in the presence of modified dextran. The biochemical composite enables the efficient synthesis of sorbitol in one pot from dextrin, cellobiose, and even cellulose. More importantly, the biochemical composite could be used repetitively many times, showing a good potential in industrial applications.

2. Experimental section

2.1. Catalyst preparation

The synthesis of biochemical composite involves the fabrication of yolk–shell structured chemical catalyst (Scheme 1A) and the integrating of the above material and enzyme (Scheme 1B). Firstly, uniform dispersing of Ru–B amorphous alloys within the porous channels of amino-functionalized mesoporous carbon nanospheres (af-mCarbon) was achieved by ultrasound-assisted incipient wetness infiltration of $(NH_4)_2RuCl_6$ onto af-mCarbon, followed by reduction with borohydride (Ru–B/af-mCarbon) [31]. Afterward, the Ru–B/af-mCarbon was coated by co-condensation of tetraethoxysilane (TEOS) and N-(amino-ethyl)-amino-propyl trimethoxy silane (APTES) in the presence of cetyltrimethylammonium bromide (CTAB), generating a core–shell structured Ru–B/af-mCarbon@CTAB/af-SiO_2, where CTAB/af-SiO_2 refers to a mesostructured CTAB/silica composite coated on the surface of the Ru–B/af-mCarbon core. Finally, the as-synthesized core–shell structured Ru–B/af-mCarbon@CTAB/af-SiO_2 was etched with hot water to achieve a yolk–shell structured configuration (Ru–B/af-mCarbon@air@af-mSiO_2). The integrating of the yolk–shell structured Ru–B/af-mCarbon@air@af-mSiO_2 and enzyme was conducted through a stepwise crosslinking method, including covalent attachment of chemical catalyst onto enzyme through a glutaraldehyde-based crosslinking technique (Ru–B/af-mCarbon@air@af-mSiO_2–A-I) and coupling of the obtained crosslinked composite with modified dextran (Ru–B/af-mCarbon@air@af-mSiO_2–A-II). More details about the catalyst preparation can be found in the Supporting Information.

2.2. Catalyst characterization

Fourier transform infrared (FTIR) spectra were obtained using a Thermo Nicolet Magna 550 spectrometer. The bulk composition

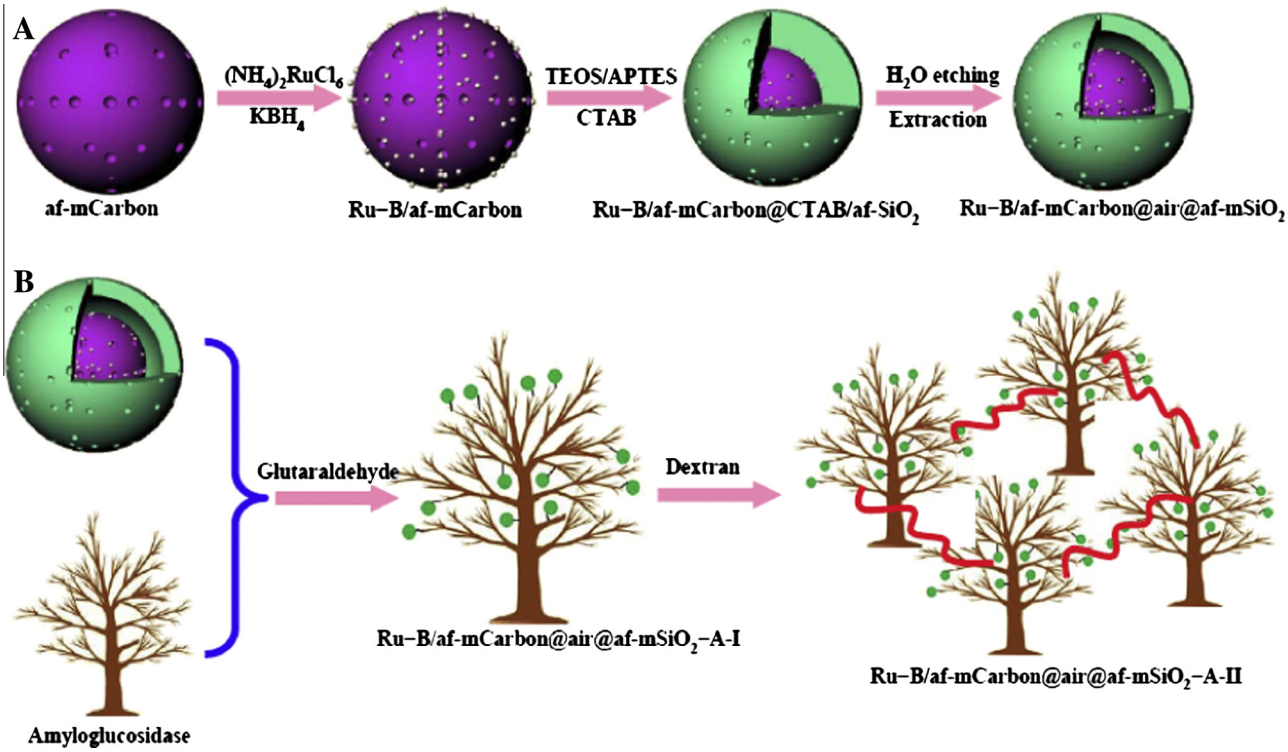

Scheme 1. Illustration of the synthesis process of (A) yolk–shell structured Ru–B/af-mCarbon@air@af-mSiO_2 and (B) biochemical composite through stepwise cross-linking technique.

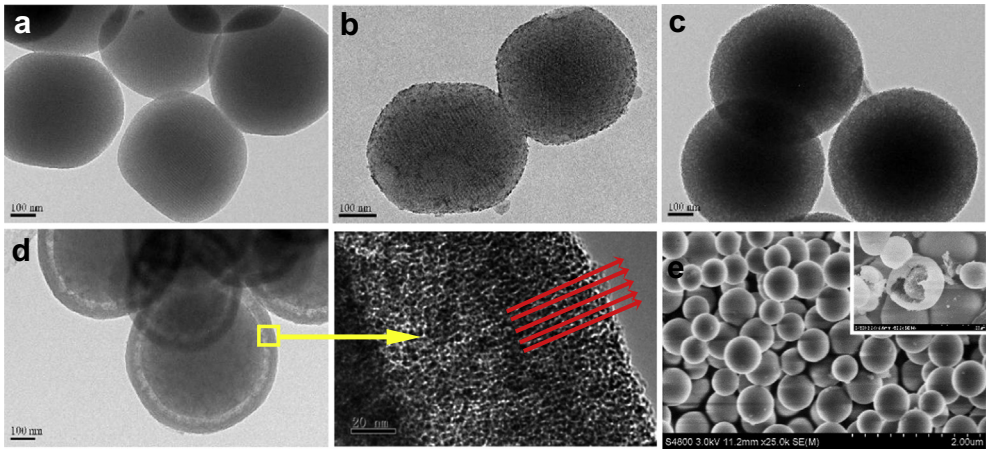

Fig. 1. TEM images of (a) af-mCarbon, (b) Ru–B/af-mCarbon, (c) Ru–B/af-mCarbon@CTAB/af-SiO_2, and (d) Ru–B/af-mCarbon@air@af-mSiO_2. (e) FESEM image of Ru–B/af-mCarbon@air@af-mSiO_2. The inset in (e) is a partially crushed sphere.

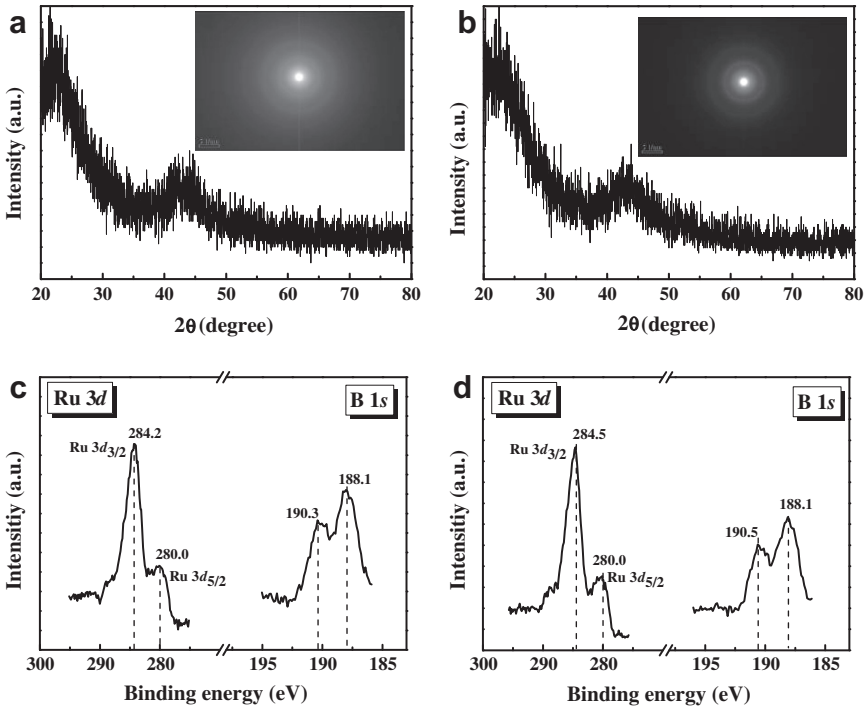

Fig. 2. Wide-angle XRD patterns of (a) Ru–B/af-mCarbon and (b) Ru–B/af-mCarbon@air@af-mSiO_2. XPS spectra of (c) Ru–B/af-mCarbon and (d) Ru–B/af-mCarbon@air@af-mSiO_2. The insets in (a) and (b) are the SAED images of the Ru–B particles.

and Ru loading were analyzed by means of inductively coupled plasma optical emission spectrometry (ICP-OES; Varian VISTA-MPX). Enzyme loading was determined by bicinchoninic acid (BCA) assay. The amorphous structure was investigated by both X-ray diffraction (XRD; Rigaku D/Max-RB with Cu Kα radiation) and selective-area electronic diffraction (SAED; JEOL JEM2100). The material shapes and morphologies were observed by both field emission scanning electron microscopy (FESEM; HITACHI S-4800) and transmission electron microscopy (TEM, JEOL JEM2100). N_2 adsorption–desorption isotherms were obtained at 77 K using a Micromeritics TriStar II apparatus. By N_2 adsorption, the Brunauer–Emmett–Teller (BET) surface area (S_{BET}) was calculated by using the multiple-point BET method in the relative pressure range of $P/P_0 = 0.05–0.2$. The pore volume and pore size distribution curve were obtained by the Barrett–Joyner–Halenda model. The surface electronic states were determined by X-ray photoelectron spectroscopy (XPS; ULVAC-PHI PHI5000 VersaProbe system using Al Kα radiation).

2.3. Catalytic performances test

In a typical experiment, the one-pot hydrolysis–hydrogenation of dextrin to sorbitol was carried out in a Parr 4848 autoclave containing Ru–B/af-mCarbon@air@af-mSiO_2–A-II (6.5 mg Ru and 25.9 mg amyloglucosidase), 0.25 g of dextrin, 25 mL of water, and 4.0 MPa of H_2 at 333 K. The reaction system was stirred vigorously (800 rpm) to eliminate the diffusion effect. The reaction mixture was sampled at intervals for product analysis on a liquid-phase chromatograph (Agilent 1200) equipped with a carbohydrate column (Shodex, SC1011) and a refractive index detector at

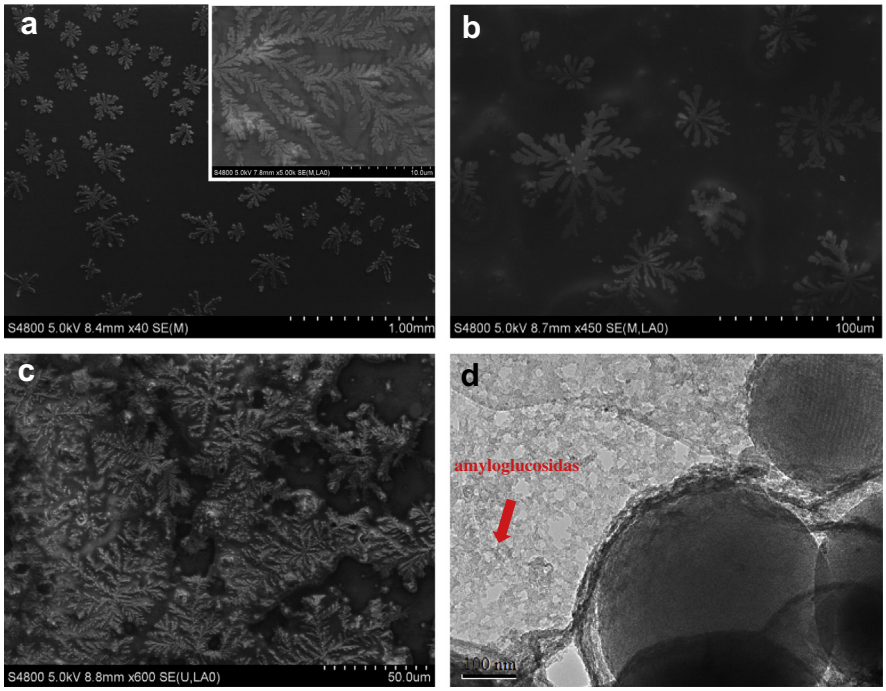

Fig. 3. FESEM images of (a) amyloglucosidase, (b) Ru–B/af-mCarbon@air@af-mSiO$_2$–A-I, and (c) Ru–B/af-mCarbon@air@af-mSiO$_2$–A-II. (d) TEM image of Ru–B/af-mCarbon@air@af-mSiO$_2$–A-II.

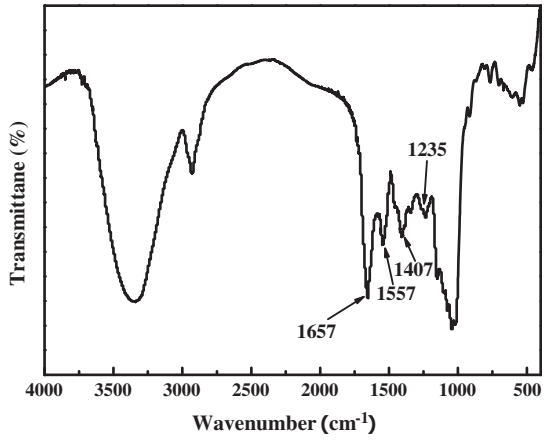

Fig. 4. FTIR spectrum of Ru–B/af-mCarbon@air@af-mSiO$_2$–A-II.

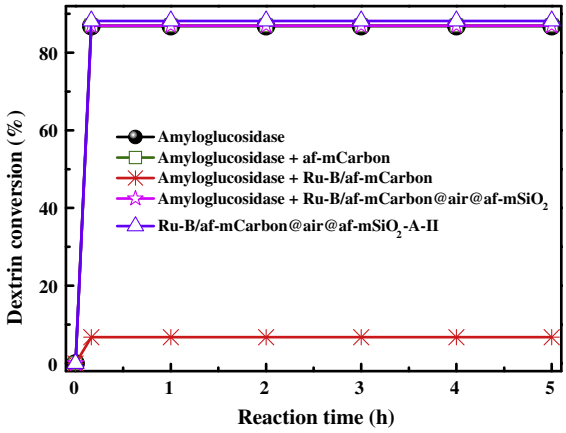

Fig. 5. Dextrin hydrolysis in different catalyst systems. Reaction conditions: dextrin (0.25 g), amyloglucosidase (20 μL), a catalyst (containing 6.5 mg Ru), water (25 mL), T = 333 K, P_{H2} = 4.0 MPa, stirring rate = 800 rpm.

333 K with water as the movable phase at 0.6 mL/min. After the mixture cooled to room temperature at the end of the reaction, the biochemical composite catalyst was separated by centrifugation and washed with deionized water for further characterization and applications. To test the catalyst durability, the used Ru–B/af-mCarbon@air@af-mSiO$_2$–A-II catalyst was centrifuged and washed thoroughly with deionized water after each run of the reaction. Then, the Ru–B/af-mCarbon@air@af-mSiO$_2$–A-II was reused with a fresh charge of dextrin for subsequent recycle run under the same reaction conditions. The supernatant was collected for BCA assay.

3. Results and discussion

3.1. Catalyst characterization

As shown in TEM image (Fig. 1a), the as-synthesized af-mCarbon is present in the form of uniform spheres with an average diameter of ~550 nm, which is similar to the pure mCarbon reported recently [23]. This demonstrates that the resulting amino-functionalized mCarbon preserves the characteristic spherical morphology of mCarbon. Meanwhile, the TEM image reveals that these nanospheres contain highly ordered mesoporous channels similar to the pure mCarbon [23]. The pore size is roughly estimated to be ~2.5 nm. N_2 physisorption experiment for the as-synthesized af-mCarbon further confirms the ordered mesoporous structure centered approximate 2.6 nm with high S_{BET} of 931 m^2 g^{-1} (Fig. S1). The successful incorporation of amino groups into the network of mCarbon was demonstrated by FTIR characterization. The FTIR spectra (Fig. S2) reveal that, besides those absorbance bands observed in the pure mCarbon, the acid-treated mCarbon displays additional absorbance bands at 1728 and 1222 cm^{-1}, corresponding to the stretching vibration of C=O bond and the bending vibration of O–H bond from the grafted –COOH groups on mCarbon [32]. Grafting TETA on the acid-treated mCarbon resulted in the remarkable decrease of O–H bending vibration and a blueshift of C=O stretching vibration to

1662 cm^{-1}, indicating the formation of the amide bond [32]. Additionally, other features should be given attention are 3041, 2930, 2849, 1453, and 1112 cm^{-1} due to N–H stretching, C–H asymmetric stretching, C–H symmetric stretching, N–H bending, and C–N stretching, respectively [33]. CO_2 temperature-program med-desorption (CO_2-TPD) was also used to confirm the incorporation of amino group into the surface of mCarbon. In case of the pure mCarbon, no CO_2 uptake was found for the used adsorption conditions (Fig. S3a); while the af-mCarbon shows pronounced CO_2 desorption peaks (Fig. S3b). All of these features indicate that the TETA have been grafted onto mCarbon successfully. Fig. 1b demonstrates that the ordered mesostructure of af-mCarbon can be well maintained after depositing Ru–B nanoparticles (NPs). Meanwhile, it can be observed that the Ru–B NPs are uniformly dispersed into the pore channels. The Ru loading was determined as 2.2 wt% by ICP analysis. From Fig. 1c, one can see that the Ru–B/af-mCarbon core is completely coated by silica shell with a thickness around 100 nm. To protect the amino functionality attached on the material, hot water (363 K) was used as etching agent for the generating of yolk–shell nanostructures in the present research. Fig. 1d reveals that, after being etched with hot water, the thickness of silica shell decreased about 20 nm, together with the formation of a space around 20 nm between the silica shell and the Ru–B/af-mCarbon core. From the FESEM image (Fig. 1e), the average diameter of the as-prepared Ru–B/af-mCarbon@air@af-mSiO_2 was estimated to be ~550 nm, which was in good line with the TEM observation. The attached FESEM image of broken Ru–B/af-mCarbon@air@af-mSiO_2 further confirms the achievement of yolk–shell structured configuration (inset in Fig. 1e). From the high-magnification TEM image of the yolk–shell structures in Fig. 1d, continuous mesochannels throughout the shell with openings at surface and radially oriented to the sphere surface can be clearly observed for the silica shell. Such a unique pore orientation is due to the perpendicular alignment of surfactant mesophases induced by the equal attractivity to polar and nonpolar species of the interface between the CTAB/silica phase and the water/ethanol solution [34–36]. The perpendicular mesoporosity in the silica shell is anticipated to increase the accessibility of the Ru–B/af-mCarbon core and thus enhancing the efficiency of mass transport. The pore size in the silica shell can be measured to be 2.6 nm by nitrogen physisorption experiment (Fig. S4).

The wide-angle XRD patterns (Fig. 2a and b) reveal that the Ru–B NPs in both the Ru–B/af-mCarbon and the Ru–B/af-mCarbon@air@af-mSiO_2 are present in the typical amorphous structure, corresponding to a broad peak at ~$2\theta = 45°$ [37,38], which is further confirmed by the consecutive diffraction halos in the attached SAED pictures [39]. The XPS spectra (Fig. 2c and d) demonstrate that all the Ru species in both the Ru–B/af-mCarbon and the yolk–shell structured Ru–B/af-mCarbon@air@af-mSiO_2 are present in metallic state, corresponding to the binding energy (BE) of 280.0 eV in Ru $3d_{5/2}$, while the B species are present in both the elemental state and the oxidized B, with BE of 188.1 and 190.5 eV in B 1*s* level. The B 1*s* BE of the elemental B exceeds that of pure B by 1.0 eV [40], suggesting the formation of Ru–B alloy in which partial electrons transfer from B to Ru. The failure in observing the BE shift of the metallic Ru can be understood by considering its relatively greater atomic weight compared with the B atom. As a result, the XRD, SAED data coupled with that of XPS, confirmed the formation of Ru–B amorphous alloy. Plenty of studies had demonstrated that Ru–B amorphous alloy has enhanced catalytic activity relative to the monometallic Ru in many reactions, including the hydrogenation of glucose to sorbitol [33]. On one hand, the unique amorphous alloy structure of Ru–B endows them with a stronger synergistic effect between Ru active sites and more highly unsaturated Ru active sites than the monometallic catalyst, which may promote the adsorption of reactants and favor hydrogenation activity [33,38]. On the other hand, the strong electronic interaction between Ru and B in the Ru–B alloys makes Ru electron enriched. The higher electron density on Ru active sites might facilitate the formation of H^- species, which would be anticipated to increase glucose hydrogenation activity [33,38].

The integrating of the yolk–shell structured Ru–B/af-mCarbon@air@af-mSiO_2 and amyloglucosidase was conducted through a stepwise crosslinking method. As shown in Fig. 3a, the free amyloglucosidase has tree-like appearance showing pinnatisect. The width of the segments can be determined as 200–300 nm. Glutaraldehyde-based crosslinking technique has proven one of the most facile methods to immobilize an enzyme on functionalized support. Therefore, glutaraldehyde was first used as crosslinker to covalently attach Ru–B/af-mCarbon@air@af-mSiO_2 onto amyloglucoamylase. The resulting Ru–B/af-mCarbon@air@af-mSiO_2–A-I preserves the characteristic tree-like shape of the free amyloglucoamylase and Ru–B/af-mCarbon@air@af-mSiO_2 particles can be found to hang on the segments of amyloglucosidase, presenting decorated tree-like structure (Fig. 3b). We presume that the crosslinking process to form Ru–B/af-mCarbon@air@af-mSiO_2–A-I was due to the interaction of glutaraldehyde with both the amino functionalities on the surface of chemical catalyst and the amino group residues in the enzyme. To further enhance the insolubility and robustness of the biochemical composite, additional coupling of Ru–B/af-mCarbon@air@af-mSiO_2–A-I was implemented by using the modified dextran as crosslinker. Under SEM, Ru–B/af-mCarbon@air@af-mSiO_2–A-II appears as aggregates (Fig. 3c), suggestive of the tying of the decorated tree-like composite with the modified dextran. From the TEM image of Ru–B/af-mCarbon@air@af-mSiO_2–A-II (Fig. 3d), the yolk–shell structured Ru–B/af-mCarbon@air@af-mSiO_2 can be also observed, demonstrating that the stepwise crosslinking was never associated with damage to the structure of chemical catalyst. Because amyloglucoamylase is extremely sensitive to the high-energy electron beam in TEM analysis, only a trail of devastation was left beside the yolk–shell structured Ru–B/af-mCarbon@air@af-mSiO_2 (marked with arrow). Furthermore, the formation of biochemical composite can be further confirmed by the FTIR spectrum. As shown in Fig. 4, Ru–B/af-mCarbon@air@af-mSiO_2–A-II displayed additional absorbance bands at 1657, 1557, 1407, and 1235 cm^{-1}, which are ascribed to the functional groups of amino acid in amyloglucoamylase. It should be noted that the C=N vibration peaks (1600–1650 cm^{-1}) as the formation of Schiff's base are covered by the characteristic peaks from amino acid groups.

More importantly, the biochemical composite, denoted as Ru–B/af-mCarbon@air@af-mSiO_2–C-II, can be also achieved from the yolk–shell structured Ru–B/af-mCarbon@air@af-mSiO_2 and cellulase by the same method, demonstrating the generality of this stepwise crosslinking strategy.

3.2. Catalytic performances

The as-prepared biochemical composites were subjected to one-pot production of sorbitol *via* hydrolysis–hydrogenation of biomass materials. We began by exploring the enzymatic efficiency of amyloglucosidase for saccharification of dextrin in different catalyst systems (Fig. 5). Note that blank run performed using amyloglucosidase accompanying with af-mCarbon delivers similar enzymatic efficiency to that of the free amyloglucosidase. Nonetheless, significant inhibiting effects on the dextrin hydrolysis activity can be observed when using amyloglucosidase in the presence of Ru–B/af-mCarbon. This implies that amyloglucosidase is easily poisoned once directly contacting with metallic Ru, in line with the results reported in our recent studies [22,23]. Hardly, any difference in the enzymatic efficiency can be found using amyloglucosidase accompanying with the yolk–shell structured Ru–B/af-mCarbon@air@af-mSiO_2, apparently owing to the protective

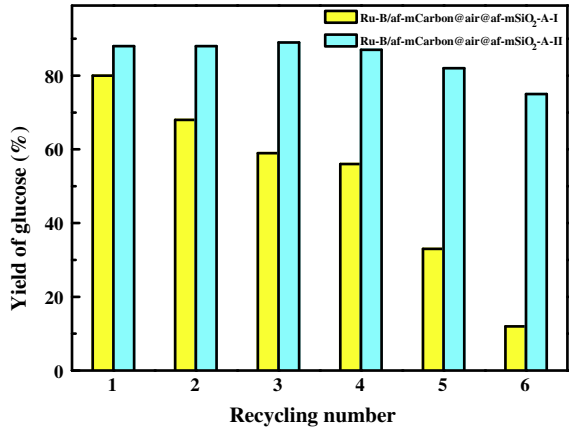

Fig. 6. Recycling test of the biochemical composites for dextrin hydrolysis. Reaction conditions: dextrin (0.25 g), biochemical composite (containing 6.5 mg Ru and 25.9 mg amyloglucosidase), water (25 mL), T = 333 K, P_{H2} = 4.0 MPa, stirring rate = 800 rpm. Each run was conducted for 5 h in recycling test. Each run was conducted for 6 h in recycling test.

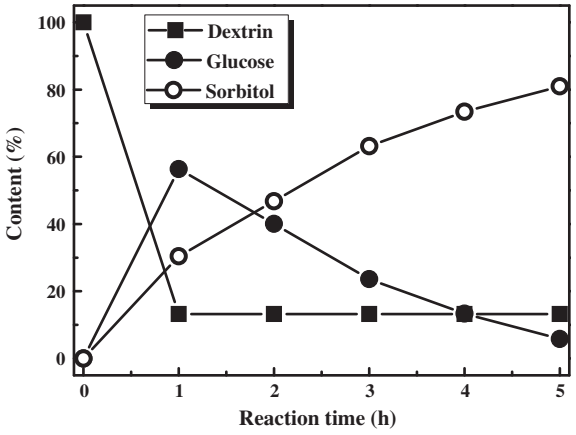

Fig. 7. Reaction profile in one-pot hydrolysis–hydrogenation of dextrin by Ru–B/af-mCarbon@air@af-mSiO$_2$–A-II. Reaction conditions: dextrin (0.25 g), 0.9 g of biochemical composite (containing 6.5 mg Ru and 25.9 mg amyloglucosidase), water (25 mL), T = 333 K, P_{H2} = 4.0 MPa, stirring rate = 800 rpm.

effect of the af-mSiO$_2$ shell that prevents amyloglucosidase from crossing over the shell to contact with the Ru-containing core. Furthermore, almost entire retention of the enzymatic efficiency for saccharification of dextrin can be observed on Ru–B/af-mCarbon@air@af-mSiO$_2$–A-II, compared to the free amyloglucosidase. This result indicates that the present stepwise crosslinking method is promising and the resulting biochemical composite is anticipated to catalyze the one-pot biomass conversion.

Industrial application of an enzyme in an immobilized form greatly relies on its stability and handling convenience [24]. Next, we first investigated the durability of the biochemical composites during the hydrolysis of dextrin. Although Ru–B/af-mCarbon@air@af-mSiO$_2$–A-I retained complete activity of the free enzyme, its stability was rather undesirable since apparent deactivation occurred during the recycling test (Fig. 6). During the hydrolysis of dextrin catalyzed by Ru–B/af-mCarbon@air@af-mSiO$_2$–A-I, we also determined the leaching amounts of amyloglucosidase by the BCA assay in the supernatants. The analysis results revealed that more than 11% and 75% of the applied enzyme leached out after the first cycle and the six cycle, respectively, suggesting that Ru–B/af-mCarbon@air@af-mSiO$_2$–A-I was soluble in water under the present conditions. In an effort to favor the stability of biochemical composite, Ru–B/af-mCarbon@air@af-mSiO$_2$–A-I was further coupled with modified dextran to afford Ru–B/af-mCarbon@air@af-mSiO$_2$–A-II. As shown in Fig. 6, the further coupled biochemical composite exhibited substantially enhanced stability under the present reaction conditions. On the basis of these observations, we can deduce that additional crosslinking of the biochemical composites would tie up them together and thus rendering them permanently insoluble and effectively preventing the leaching of enzyme while maintaining the enzymatic efficiency.

The as-prepared insoluble and robust Ru–B/af-mCarbon@air@af-mSiO$_2$–A-II was then subjected to one-pot conversion of dextrin to sorbitol (Scheme 2). As shown in Fig. 7, the enzyme catalyzed

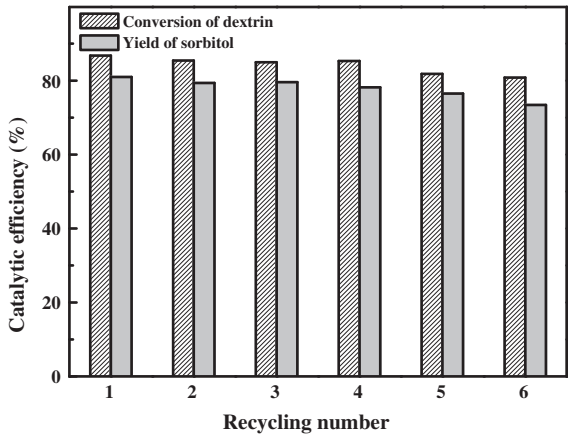

Fig. 8. Recycling test of Ru–B/af-mCarbon@air@af-mSiO$_2$–A-II for one-pot hydrolysis–hydrogenation of dextrin. Reaction conditions: dextrin (0.25 g), 0.9 g of biochemical composite (containing 6.5 mg Ru and 25.9 mg amyloglucosidase), water (25 mL), T = 333 K, P_{H2} = 4.0 MPa, and stirring rate = 800 rpm. Each run was conducted for 5 h in recycling test.

saccharification of dextrin to release glucose molecules rapidly. The produced glucose would diffuse through the af-mSiO$_2$ shell in Ru–B/af-mCarbon@air@af-mSiO$_2$, followed by the hydrogenation to the final product, sorbitol, over the catalytically active cores. Our observations suggest that the mesoporous silica shell in Ru–B/af-mCarbon@air@af-mSiO$_2$ plays a key role in conducting the one-pot dextrin conversion. On one hand, af-mSiO$_2$ shell blocks the big dextrin molecules and other colloidal substances (100–1000 nm) stemmed from the dextrin hydrolysis out of the yolk–shell nanostructures, efficiently protecting the Ru active sites from being covered. On the other hand, af-mSiO$_2$ shell allows the produced glucose (~1 nm) from dextrin hydrolysis diffuse across

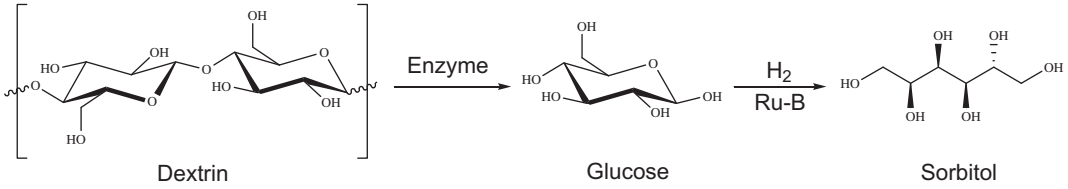

Scheme 2. One-pot hydrolysis–hydrogenation of dextrin to sorbitol by merger of enzymatic and metallic catalysis.

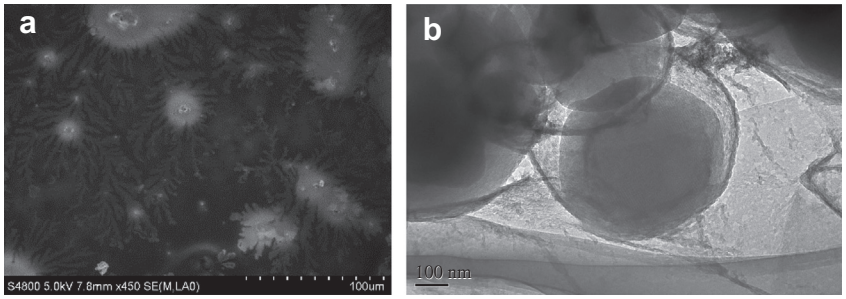

Fig. 9. (a) FESEM and (b) TEM images of the Ru–B/af-mCarbon@air@af-mSiO$_2$–A-II after being reused for 6 times.

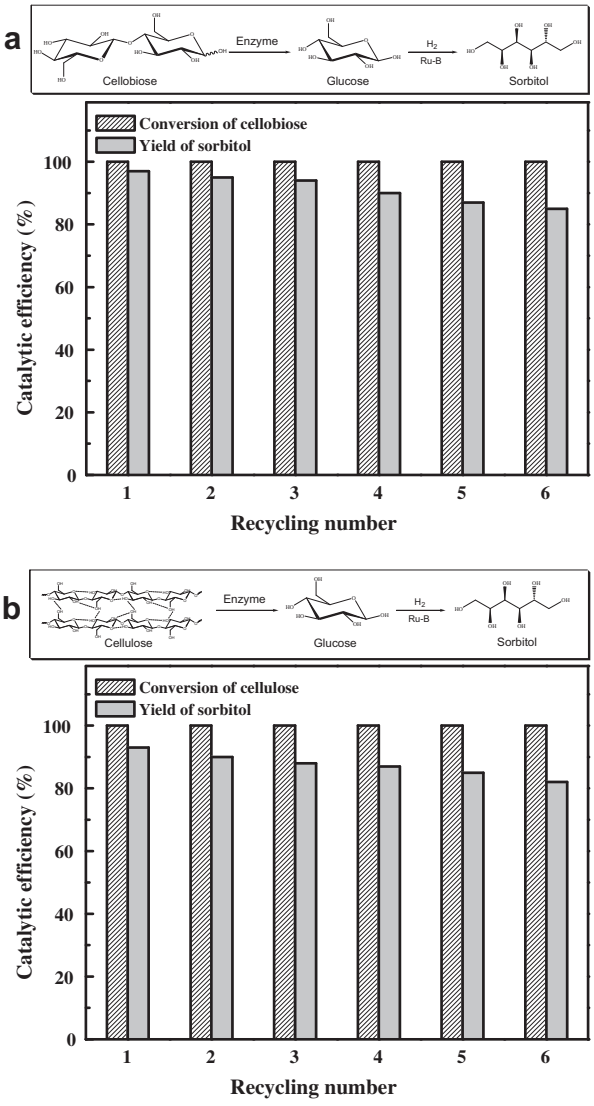

Fig. 10. Recycling test of Ru–B/af-mCarbon@air@af-mSiO$_2$–C-II for one-pot hydrolysis–hydrogenation of (a) cellobiose and (b) cellulose. Reaction conditions: cellobiose or cellulose (0.1 g), 0.68 g of biochemical composite (containing 2.6 mg Ru and 0.33 g cellulase), water (20 mL), T = 333 K, P_{H2} = 4.0 MPa, and stirring rate = 800 rpm. Each run was conducted for 6 h in recycling test.

the shell and then be hydrogenated to sorbitol over the Ru–B/af-mCarbon core. Notably, the catalytic efficiency of the present biochemical composite exceeds those we reported recently. For example, the present biochemical composite enables the one-pot dextrin conversion to proceed at moderate temperature (333 K vs. 348 K [22] and 343 K [23]). Additionally, only a shorter time (5 h) in the present system is needed to obtain the similar sorbitol yield to the recent results (7 h [22] and 6 h [23]). As demonstrated above, the dextrin hydrolysis efficiency can be retained entirely in Ru–B/af-mCarbon@air@af-mSiO$_2$–A-II, the enhanced catalytic efficiency of the present biochemical composite should be thanks to the superior glucose hydrogenation activity of the Ru–B/af-mCarbon@air@af-mSiO$_2$ to the previous systems. On one hand, the amino groups grafted in mCarbon serve as anchor points [33], favoring the uniform dispersion of Ru–B. On the other hand, the amino groups enhance the concentration of ionized glucose species *via* abstracting the proton from the anomeric hydroxyl group in glucose [41]. Beenackers et al. [42] showed that, upon generation of the glucose anion, it was susceptible to attack by hydrogen adsorbed dissociatively on the neighboring metal sites.

We also discovered another desirable attribute of our process: handling convenience and the stability. Ru–B/af-mCarbon@air@af-mSiO$_2$–A-II could be easily separated from the reaction solution *via* centrifugation and used repetitively at least for 6 times with only 9% decrease of sorbitol yield during the one-pot hydrolysis–hydrogenation of dextrin (Fig. 8), showing its superiority over the simple combination of the free amyloglucosidase and the yolk–shell structured chemical catalysts [22,23]. During the recycling test, the dextrin conversion decreased by 7% after being used 6 times. Accordingly, the slight decrease in sorbitol yield after 6 cycles should be attributed to the partial lost in enzymatic efficiency for saccharification of dextrin. The FESEM and TEM images (Fig. 9) showed that both the decorated tree-like structure of the biochemical composite and the yolk–shell structure morphology of the chemical catalyst were still present after 6 cycles. However, the leaching amount of amyloglucosidase was determined as 5% by the BCA assay in the supernatant, demonstrating that leaching of enzyme might be the main factor responsible for the decrease in efficiency.

Finally, further investigations of the generality of the present strategy revealed that one-pot synthesis of sorbitol can be also achieved *via* hydrolysis–hydrogenation of cellobiose and even cellulose by Ru–B/af-mCarbon@air@af-mSiO$_2$–C-II with 6 cycles of successive use (Fig. 10). From the viewpoint of practical applications, transforming the inedible biomass materials into valuable platform chemicals is more economical issue. Therefore, further optimization may eventually make the approach industrially viable for the conversion of non-food biomass into sorbitol as a renewable platform chemical.

4. Conclusions

In summary, our research provides a paradigm for the utility of crosslinking technique for the integrating of chemical catalyst and the macromolecular enzyme into biochemical composite. The recyclable biochemical composite can be used to convert biomass

materials into sorbitol in high efficiency. This one-pot process may find important applications for the efficient production of renewable platform chemicals from biomass materials without intermediate purification. Moreover, this strategy can potentially be extended to other biochemical composites with different composition and thus versatile functions.

Acknowledgments

This work is supported by the National Natural Science Foundation of China (21273149), PCSIRT (IRT1269), the Program for New Century Excellent Talents in University (NCET-11-1052), the Shanghai Science & Technology and Education Committee (11JC1408900, 12490502800, 10SG41), and State Key Laboratory of Chemical Engineering (SKL-ChE-14C05).

Appendix A. Supplementary material

Supplementary data associated with this article can be found, in the online version, at http://dx.doi.org/10.1016/j.jcat.2015.04.021.

References

[1] A. Corma, S. Iborra, A. Velty, Chem. Rev. 107 (2007) 2411.
[2] R. Rinaldi, F. Schüth, Energy Environ. Sci. 2 (2009) 610.
[3] D.A. Simonetti, J.A. Dumesic, Catal. Rev. – Sci. Eng. 51 (2009) 441.
[4] J.C. Serrano-Ruiz, J.A. Dumesic, Energy Environ. Sci. 4 (2011) 83.
[5] M. Besson, P. Gallezot, C. Pinel, Chem. Rev. 114 (2014) 1827.
[6] T. Werpy, G. Peterson, Top Value Added Chemicals from Biomass: Results of Screening for Candidates from Sugars and Synthesis Gas, vol. 1, US Department of Energy, Energy Efficiency and Renewable Energy, Battelle, Richland, WA. <http://www1.eere.energy.gov/biomass/pdfs/35523.pdf>.
[7] W.S. Fedor, J. Millar, A.J. Accola, Ind. Eng. Chem. 52 (1960) 282.
[8] W.M. Kruse, L.W. Wright, Carbohydr. Res. 64 (1978) 293.
[9] P. Gallezot, P.J. Cerino, B. Blanc, G. Fleche, P. Fuertes, J. Catal. 146 (1994) 93.
[10] H. Li, H.X. Li, J.F. Deng, Catal. Today 74 (2002) 53.
[11] B. Kusserow, S. Schimpf, P. Claus, Adv. Synth. Catal. 345 (2003) 289.
[12] S. Schimpf, C. Louis, P. Claus, Appl. Catal., A 356 (2009) 112.
[13] V.N. Sapunov, M.Y. Grigoryev, E.M. Sulman, M.B. Konyaeva, V.G. Matveeva, J. Phys. Chem. A 117 (2013) 4073.
[14] D. Yankov, E. Dobreva, V. Beschkov, E. Emanuilova, Enzyme Microb. Technol. 8 (1986) 665.
[15] R. Hoover, Food Rev. Int. 16 (2000) 369.
[16] J. Kadokawa, Chem. Rev. 111 (2011) 4308.
[17] M. Katz, E.E. Reese, Appl. Microbiol. 12 (1968) 419.
[18] A. Bruggink, R. Schoevaart, T. Kieboom, Org. Process Res. Dev. 7 (2003) 622.
[19] C. Simons, U. Hanefeld, I.W.C.E. Arends, T. Maschmeyer, R.A. Scheldon, Top. Catal. 40 (2006) 35.
[20] M.J. Climent, A. Corma, S. Iborra, Chem. Rev. 111 (2011) 1072.
[21] N. Ren, Y.H. Yang, J. Shen, Y.H. Zhang, H.L. Xu, Z. Gao, Y. Tang, J. Catal. 251 (2007) 182.
[22] L. Xu, W. Wei, H.X. Li, H. Li, ACS Catal. 4 (2014) 251.
[23] W. Wei, Y. Zhao, S.C. Peng, H.Y. Zhang, Y.P. Bian, H.X. Li, H. Li, ACS Appl. Mater. Interfaces 6 (2014) 20851.
[24] R.A. Sheldon, Adv. Synth. Catal. 349 (2007) 1289.
[25] R. Torres, B.C.C. Pessela, C. Mateo, C. Ortiz, M. Fuentes, J.M. Guisan, R. Fernandez-Lafuente, Biotechnol. Prog. 20 (2004) 1297.
[26] H. Kamal, G.M. Sabry, S. Lotfy, N.M. Abdallah, J. Rosiak, E.A. Hegazy, J. Macromol. Sci. 45 (2008) 65.
[27] A. Panek, O. Pietrow, J. Synowiecki, Strach 64 (2012) 1003.
[28] A. Tanriseven, Z. Ölçer, J. Synowiecki, Biochem. Eng. J. 39 (2008) 430.
[29] R.A. Persichetti, N.L.S. Clair, J.P. Griffith, M.A. Navia, A.L. Margolin, J. Am. Chem. Soc. 117 (1995) 2732.
[30] S. Talekar, S. Desai, M. Pillai, N. Nagavekar, S. Ambarkar, S. Surnis, M. Ladole, S. Nadar, M. Mulla, RSC Adv. 3 (2013) 2265.
[31] Y. Wang, L. Xu, L. Xu, H.X. Li, H. Li, Chin. J. Catal. 34 (2013) 1027.
[32] J. Chen, M.A. Hamon, H. Hu, Y.S. Chen, A.M. Rao, P.C. Eklund, R.C. Haddon, Science 282 (1998) 95.
[33] S.L. Wang, W. Wei, Y. Zhao, H.X. Li, H. Li, Catal. Today, http://dx.doi.org/10.1016/j.cattod.2014.07.039.
[34] B. Tan, S.E. Rankin, J. Phys. Chem. B 108 (2004) 20122.
[35] S.B. Yoon, J.Y. Kim, J.H. Kim, Y.J. Park, K.R. Yoon, S.K. Park, J.S. Yu, J. Mater. Chem. 17 (2007) 1758.
[36] Y.H. Deng, Y. Cai, Z.K. Sun, J. Liu, C. Liu, J. Wei, W. Li, C. Liu, Y. Wang, D.Y. Zhao, J. Am. Chem. Soc. 132 (2010) 8466.
[37] Y. Pei, G.B. Zhou, N. Luan, B.N. Zong, M.H. Qiao, F. Tao, Chem. Soc. Rev. 41 (2012) 81409.
[38] H. Li, W. Wei, Y. Zhao, H.X. Li, Catalysis 27 (2015) 144.
[39] S. Klein, J.A. Martens, R. Parton, K. Vercruysse, P.A. Jacobs, W.F. Maier, Catal. Lett. 38 (1996) 209.
[40] H. Li, H.X. Li, W.L. Dai, W.J. Wang, Z.G. Fang, J.F. Deng, Appl. Surf. Sci. 152 (1999) 25.
[41] G. de Wit, J.J. de Vlieger, A.C.K. Dalen, R. Heus, R. Laroy, A.J. Van Hengstum, A.P.G. Kieboom, H. Van Bekkum, Carbohydr. Res. 91 (1981) 125.
[42] J.A.W.M. Beenackers, B.F.M. Kuster, H.S. Van der Baan, Carbohydr. Res. 140 (1985) 169.